

# Effect of dipolar interactions and DC magnetic field on the specific absorption rate of an array of magnetic nanoparticles

J.-L. Déjardin<sup>1, a)</sup>, F. Vernay<sup>1, b)</sup>, M. Respaud<sup>2, c)</sup> and H. Kachkachi<sup>1d)</sup>

<sup>1</sup>Laboratoire PROMES-CNRS (UPR-8521) & Université de Perpignan Via Domitia, Rambla de la thermodynamique, Tecnosud, 66100 Perpignan, FRANCE.

<sup>2</sup>Laboratoire de Physique et Chimie des Nano-Objets, INSA, 135 Avenue de Rangueil, 31077 Toulouse, FRANCE

(Dated: July 21, 2018)

We address the issue of inter-particle dipolar interactions in the context of magnetic hyperthermia. More precisely, the main question dealt with here is concerned with the conditions under which the specific absorption rate is enhanced or reduced by dipolar interactions. For this purpose, we propose a theory for the calculation of the AC susceptibility, and thereby the specific absorption rate, for a monodisperse two-dimensional assembly of nanoparticles with oriented anisotropy, in the presence of a DC magnetic field, in addition to the AC magnetic field. We also study the competition between the dipolar interactions and the DC field, both in the transverse and longitudinal configurations. In both cases, we find that the specific absorption rate has a maximum at some critical DC field that depends on the inter-particle separation. In the longitudinal setup, this critical field falls well within the range of experiments.

## I. INTRODUCTION

Today magnetic hyperthermia is one of the most promising applications of magnetic nanoparticles. This is an experimental medical treatment of cancer that has recently attracted numerous investigations from the physics perspective.<sup>1-8</sup> It consists in injecting in tumor cells magnetic nanoparticles whose magnetization is then excited by an external AC magnetic field into a fast switching motion. As a consequence, there is an elevation of temperature of several Kelvins inside the cells that eventually leads to their destruction. One of the most relevant quantities to the efficiency of this process is what is called the *specific absorption rate* (SAR), which is defined as the power absorbed by a magnetic sample subjected to an external AC field

$$\text{SAR} = \Re \left( \frac{\mu_0 \omega}{2\pi} \oint_{\text{cycle}} \mathbf{M} \cdot d\mathbf{H}_{\text{ac}} \right). \quad (1)$$

The integration here is performed over one cycle of the magnetic field and gives the energy dissipation per cycle.  $\mathbf{M}$  is the sample's magnetization and  $\omega$  the angular frequency of the AC magnetic field  $\mathbf{H}_{\text{AC}} = H_0 \exp(i\omega t) \mathbf{e}_x$ . By integration of Eq. (1), it can be shown within the framework of linear-response theory that the SAR is directly proportional to the imaginary component of the AC susceptibility  $\chi''(\omega)$ <sup>9,10</sup>. More precisely, we have

$$\text{SAR} = \frac{\mu_0 \omega}{2\pi} H_0^2 \chi''(\omega). \quad (2)$$

See also Ref. 11 for a detailed derivation of the related volumetric power dissipation.

Hence, computing the SAR for an assembly of nanoparticles can be achieved upon obtaining its AC susceptibility. If we denote by  $\chi_{\text{eq}}$  the equilibrium susceptibility and by  $\Gamma$  the relaxation rate (the inverse longitudinal relaxation time  $\tau = \Gamma^{-1}$ ), the AC susceptibility may be computed according to the Debye model<sup>12,13</sup>

$$\chi(\omega) = \frac{\chi_{\text{eq}}}{1 + i\omega\Gamma^{-1}}. \quad (3)$$

Therefore, upon computing the equilibrium susceptibility  $\chi_{\text{eq}}$  and the relaxation rate  $\Gamma$  of the assembly, in the presence of dipolar interactions (DI) and a DC magnetic field, we can investigate the effects of the latter two contributions on the SAR. This is the main task of the present work. Accordingly, we will study the effects of dipolar interactions and DC magnetic field on the SAR of a mono-disperse assembly of magnetic nanoparticles arranged in a regular super-lattice. Our main objective here is to investigate the conditions regarding DI and DC field under which the SAR may be enhanced. Magnetic hyperthermia makes use of a kind of ferrofluid, *i.e.* an ensemble of (ferro) magnetic nanoparticles floating in a fluid. In this work we consider instead a solid matrix in which the nanoparticles are embedded and spatially arranged. However, in order to investigate the qualitative features of the SAR as a function of the assembly concentration and magnetic DC field, we resort to a simple analytical formalism which still captures the main behavior with respect to these two parameters.

The article is organized as follows: in the next Section we present our model and hypotheses. Section III is devoted to the calculation of the AC susceptibility within the framework of the Debye model. This requires the calculation of the equilibrium susceptibility as well as the relaxation rate. We finally obtain an expression of the SAR as a function of the assembly concentration  $C_v$  and applied DC field. The article ends with our concluding remarks and perspectives.

<sup>a)</sup>Electronic mail: [dejardin@univ-perp.fr](mailto:dejardin@univ-perp.fr)

<sup>b)</sup>Electronic mail: [francois.vernay@univ-perp.fr](mailto:francois.vernay@univ-perp.fr)

<sup>c)</sup>Electronic mail: [marc.respaud@insa-toulouse.fr](mailto:marc.respaud@insa-toulouse.fr)

<sup>d)</sup>Electronic mail: [hamid.kachkachi@univ-perp.fr](mailto:hamid.kachkachi@univ-perp.fr)

## II. MODEL AND HYPOTHESES

We consider a monodisperse assembly of  $\mathcal{N}$  single-domain nanoparticles with oriented (effective) uniaxial anisotropy, each having a magnetic moment  $\mathbf{m}_i = m_i \mathbf{s}_i$ ,  $i = 1, \dots, \mathcal{N}$  of magnitude  $m$  and direction  $\mathbf{s}_i$ , with  $|\mathbf{s}_i| = 1$ . For the sake of simplicity, and without loss of generality, we focus on a simple geometry: the assembly is organized into a simple cubic two-dimensional super-lattice of parameter  $a$ . Indeed, the approach adopted here can easily be extended to more general situations upon computing the super-lattice sums of the corresponding geometry and spatial configuration. This method is general and the standard sums involved in such calculations have already been introduced in similar contexts where the dipolar interactions have to be taken into account<sup>14,15</sup>. Setting up the assembly in the  $xy$  plane, each nanoparticle of volume  $V$  is attributed an (effective) uniaxial anisotropy constant  $K_{\text{eff}}$  with an easy-axis in the  $z$  direction. Indeed, even if the nanoparticles are modeled here as spheres, we assume that asperities on their outer shell and related surface effects may induce an effective easy axis for their resultant magnetic moment. Furthermore, we assume that these easy axes are all pointing in the  $z$  direction. The present calculations can, of course, be extended so as to include volume and anisotropy-easy axis distributions using a fully numerical approach. However, as stated earlier, in this work we would like to focus on the qualitative behavior of the SAR in the presence of DI and a DC magnetic field and derive simple formulae for practical use.

For later use we introduce the (dimensionless) anisotropy-energy barrier  $\sigma = K_{\text{eff}}V/k_B T$ .  $K_{\text{eff}}$  is considered to be the largest energy scale of our model (*i.e.*  $\sigma \gg 1$ ), meaning that the anisotropy barrier is the dominant term in the expression of the energy. This limit applies to most hyperthermia experiments (at temperature  $T \simeq 318\text{K}$ ) on iron-cobalt nanoparticles of volume  $V \sim 5.23 \times 10^{-25}\text{m}^3$  (*i.e.* spheres of radius  $R = 5\text{ nm}$ ) with an effective anisotropy constant  $K_{\text{eff}} \sim 4.5 \times 10^4\text{J.m}^{-3}$ . Indeed, in this case one has  $\sigma \simeq 5.4$ . These assumptions also apply to the various systems investigated in the literature<sup>16–19</sup>.

The energy of a magnetic moment  $\mathbf{m}_i$  interacting with the other moments of the assembly and subjected to an external DC magnetic field  $\mathbf{H}_{\text{ex}} = H_{\text{DC}}\mathbf{e}_z$ , reads (after multiplying by  $-\beta \equiv -1/k_B T$ )

$$\mathcal{E}_i = \mathcal{E}_i^{(0)} + \mathcal{E}_i^{\text{DI}}, \quad (4)$$

where

$$\mathcal{E}_i^{(0)} = x \mathbf{s}_i \cdot \mathbf{e}_z + \sigma (\mathbf{s}_i \cdot \mathbf{e}_z)^2 \quad (5)$$

is the energy of a single (noninteracting) nanoparticle located at site  $i$ . This includes the Zeeman and anisotropy terms, with  $x = \beta m H_{\text{DC}}$ . The second term in Eq. (4) is

the contribution from the long-range DI,

$$\mathcal{E}_i^{\text{DI}} = \xi \sum_{j < i} \mathbf{s}_i \cdot \mathcal{D}_{ij} \cdot \mathbf{s}_j, \quad (6)$$

with the usual tensor

$$\mathcal{D}_{ij} \equiv \frac{1}{r_{ij}^3} (3\mathbf{e}_{ij}\mathbf{e}_{ij} - 1) \quad (7)$$

where  $\mathbf{r}_{ij} = \mathbf{r}_i - \mathbf{r}_j$ ,  $r_{ij} = |\mathbf{r}_{ij}|$  and  $\mathbf{e}_{ij} = \mathbf{r}_{ij}/r_{ij}$  a unit vector along the link  $i \rightarrow j$ . In dimensionless units the DI coefficient  $\xi$  reads

$$\xi = \left(\frac{\mu_0}{4\pi}\right) \left(\frac{m^2/a^3}{k_B T}\right). \quad (8)$$

Alternatively, the DI can be expressed as the result of the DI field  $\mathbf{\Xi}_i$  acting on  $\mathbf{m}_i$  with

$$\mathbf{\Xi}_i = \xi \sum_{j \neq i} \mathcal{D}_{ij} \cdot \mathbf{s}_j. \quad (9)$$

The main purpose of our investigation is to derive (semi-)analytical formulae that account for the effect of DI and DC field on the SAR. Accordingly, we limit the present study to low particle concentrations (*i.e.*  $\xi \ll 1$ ) since then we can use perturbation theory to investigate the behavior of the SAR upon varying  $\xi$  and  $x$ .

Now, a word is in order regarding Debye's formula (3). In Ref. 20 the contribution of DI to the relaxation rate  $\Gamma$  was obtained in the adiabatic approximation. More precisely, for an ensemble of weakly coupled magnetic moments, one assumes that there are mainly two time scales:

- the “single-particle” time scale  $\tau_s \sim 1/\gamma H_K$ , where  $\gamma$  is the gyromagnetic factor and  $H_K$  the anisotropy field of the particle.  $\tau_s$  is the (intrinsic) characteristic time of the dynamics of an individual magnetic moment,
- the “collective” time scale  $\tau = \Gamma^{-1}$  that corresponds to the dynamics of the “soft” collective state induced by (weak) DI in the whole assembly.

Thus, in the adiabatic approximation one assumes that  $\tau \gg \tau_s$ , which means that because of the weak DI, what is happening at the level of individual moments is conveyed with delay to the other moments and eventually to the whole assembly. Equivalently, this implies that when the dynamics of an individual magnetic moment is probed and the relaxation rate is being measured, one assumes that the other moments are “frozen in time” and exert only a static “molecular” field on the moment considered. Hence, the latter is subject to a static effective field due to DI, in addition of course to the anisotropy and Zeeman fields. In conclusion, in the present approach, it is understood that the collective dynamics of the system is assumed to be dominated by a “slow” mode corresponding to one (longitudinal) relaxation time. This comes out

as a correction to the Debye formula and which is taken into account in the present work by a DI correction of the equilibrium susceptibility and the longitudinal relaxation time. This is done in analogy with various works on the extensions of Debye's model in the context of dielectric relaxation. Indeed, the simplest model of orientational relaxation is that of rotational diffusion first proposed by Debye<sup>21</sup> in which rigid molecules diffuse independently. Zwanzig<sup>22</sup> [see also Ref. 23] later investigated how DI affect this model on a rigid cubic lattice. It was shown that, to first-order in concentration (or DI coefficient  $\xi$ ), one obtains only one (longitudinal) relaxation time shifted from the molecular relaxation time by some correction factor that depends on the density of the lattice, with a very good agreement with Debye's formula. The correction factor vanishes at vanishing density. The high-order corrections to the Debye formula are responsible for new relaxation times that become relevant at much higher frequencies, *e.g.* in FMR measurements.

### III. AC SUSCEPTIBILITY

AC susceptibility can be written as  $\chi(x, \sigma, \xi, \omega) = \chi' - i\chi''$  with its real and imaginary components given by

$$\chi' = \chi^{\text{eq}} \frac{1}{1 + \eta^2}, \quad \chi'' = \chi^{\text{eq}} \frac{\eta}{1 + \eta^2}, \quad (10)$$

with  $\chi^{\text{eq}}$  being the equilibrium susceptibility, *i.e.* the response of the magnetic system to the static magnetic DC field  $\mathbf{H}_{\text{ex}}$ . On the other hand, the AC susceptibility is the response of the system to  $\mathbf{H}_{\text{AC}}$ , the AC magnetic field. In the present work, we remain within the linear-response regime since  $H_0$  is assumed to be too small to change the energy states of the magnetic system. For this reason,  $\mathbf{H}_{\text{AC}}$  does not need to be included in the Hamiltonian that is used for determining the equilibrium states of the system. The parameter  $\eta$  in Eq. (10) is given by  $\eta = \omega\Gamma^{-1}$  where  $\Gamma$  is the relaxation rate associated with the magnetization switching between its minimal-energy orientations.

In the presence of (weak) DI, in Refs. 15 and 24,  $\chi^{\text{eq}}$

was shown to be given by

$$\chi^{\text{eq}} \simeq \chi_{\text{free}}^{\text{eq}} + \tilde{\xi} \chi_{\text{int}}^{\text{eq}}, \quad (11)$$

where  $\tilde{\xi} \equiv \xi \mathcal{C}^{(0,0)}$ , with  $\mathcal{C}^{(0,0)}$  being a lattice sum that can be expressed in terms of the assembly demagnetizing factor along  $z$  [see Section V B]. For instance, for the specific case of a square sample, as shown in Fig. 1, the lattice sum is given by (in the thermodynamic limit)  $\mathcal{C}^{(0,0)} \simeq -9$ , whereas it is positive for a prolate sample of the form  $L \times L \times 2L$  for which  $\mathcal{C}^{(0,0)} \simeq 1.7$ .

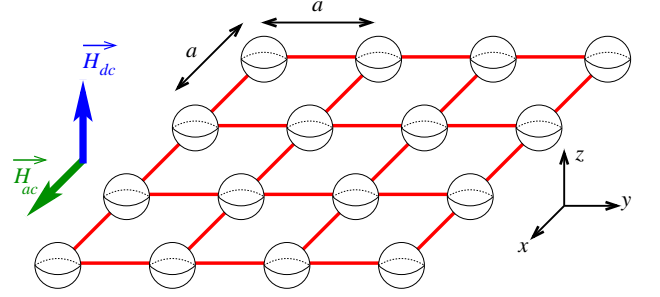


Figure 1. 2D assembly of nano-spheres on a square superlattice of parameter  $a$ . The external DC field is applied along the  $z$ -axis, the AC field lies within the  $xy$ -plane. We assume the assembly to be monodisperse with all anisotropy easy axes oriented in the  $z$  direction.

$\chi_{\text{free}}^{\text{eq}}$  and  $\chi_{\text{int}}^{\text{eq}}$  represent the contributions to the linear equilibrium susceptibility without DI and with DI, respectively. Their explicit derivation can be found in Refs. 14 and 24. Here we only report the main result for the longitudinal DC field case

$$\chi_{\text{free}}^{\text{eq}} = \frac{\mu_0 m^2}{k_B T} \left[ 1 - \frac{1}{\sigma} - \left( 1 - \frac{2}{\sigma} \right) x^2 \right], \quad (12)$$

$$\chi_{\text{int}}^{\text{eq}} = \frac{\mu_0 m^2}{k_B T} \left[ 1 - \frac{2}{\sigma} - 4 \left( 1 - \frac{3}{\sigma} \right) x^2 \right]. \quad (13)$$

Note that these two expressions are valid for  $x \lesssim 0.5$ . For larger values of  $x$ , we must use the expressions given in Eqs. (3.85) & (3.39) of Ref. 12, with  $h = x/2\sigma$ . In the present notations, these are rewritten as follows

$$\chi_{\text{free,GP}}^{\text{eq}} \simeq \frac{\mu_0 m^2}{k_B T} \frac{1}{(\cosh x - h \sinh x)^2} \times \left\{ (1 - h^2) - \frac{1}{\sigma} + \frac{1}{8\sigma^2} \left[ 1 - \frac{(1 + 6h^2 + h^4) \cosh(2x) - 4h(1 + h^2) \sinh(2x)}{(1 - h^2)^2} \right] \right\}, \quad (14)$$

$$\chi_{\text{int,GP}}^{\text{eq}} \simeq \frac{\mu_0 m^2}{k_B T} \frac{1}{2} \frac{\partial^2}{\partial x^2} \left\{ \tanh x \left[ 1 - \frac{1}{2\sigma} \left( 1 + \frac{2x}{\sinh(2x)} \right) - \frac{1}{8\sigma^2} \left( 4 - x \frac{\sinh(2x) - 2x}{\cosh^2 x} \right) \right] \right\}^2. \quad (15)$$

The difference between  $\chi^{\text{eq}}$  in Eqs. (12, 13) and Eqs.

(14, 15) is shown in Fig. 2. Their comparison allows us

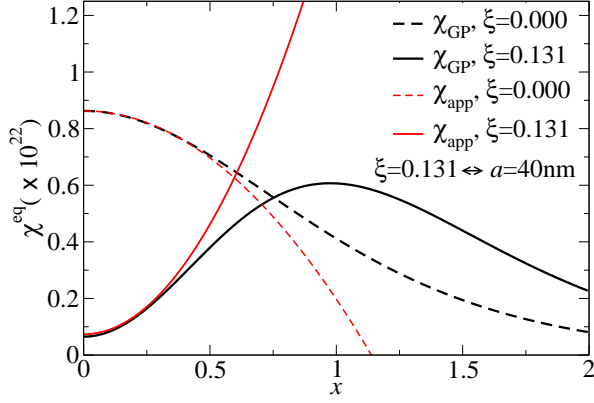


Figure 2. Linear susceptibility  $\chi^{\text{eq}}$  as a function of the (reduced) longitudinal DC field  $x$  in the absence of DI (dashed lines  $\xi = 0$ ) and in the presence of DI (continuous lines  $\xi = 0.131$ , *i.e.* with super-lattice parameter  $a = 40$  nm). The curves in black are plots of Eqs. (14,15), of Ref. 12 (GP stands for Garcia-Palacios), while the curves in red are plots of the expressions in Eqs. (12,13).

to establish the validity of the approximate expressions in Eqs. (12, 13). Note in passing that all these expressions are only valid in the limit  $\sigma \ll 1$ , which is relevant for the specific case of hyperthermia. More general expressions can be obtained if one rederives the equilibrium susceptibility from exact expressions of the magnetization as given in Refs. 25 and 26. We have checked that the  $\frac{1}{\sigma}$ -series expansion of the latter gives the same expressions as used here. The main feature that appears in the presence of DI is clearly shown by the black curves in Fig. 2: the competition between on one hand, the DI that tend to maintain the magnetization within the  $xy$ -plane, and on the other, the external DC field together with anisotropy that tend to align the magnetic moments along the  $z$ -direction, leads to a nonmonotonic behavior of  $\chi^{\text{eq}}$  with a maximum at an external DC field  $x_m \sim 0.9$ . In the limit of high anisotropy-energy barrier, namely  $\sigma \gg 1$ , this maximum can be analytically obtained; it only depends on the DI parameter  $\xi$  as follows

$$x_m = \text{Arcsech} \left[ \frac{1}{\sqrt{3}} \sqrt{1 - \frac{1}{2\xi}} \right]. \quad (16)$$

For the present case, with  $\xi = 0.131$  and lattice sum  $\mathcal{C}^{(0,0)} = -9$  (*i.e.*  $\xi = -0.972$ ), we obtain  $x_m \simeq 0.875$  which is in agreement with the result in Fig. 2.

The remaining task in the calculation of the AC susceptibility (10) is to compute the relaxation rate, or the (dimensionless) relaxation time  $\eta$ . For a single (noninteracting) particle the relaxation rate  $\Gamma_0$ , in a longitudinal DC field, is given by the Néel-Brown formula<sup>27</sup>. The longitudinal relaxation rate given by Néel-Brown formula is valid for any  $\sigma$  as long as the two-well character of the energy potential is preserved. Indeed, the relaxation rate computed within Brown's or Langer's approach is based on the notion of escape rate (or first-passage time) from a

metastable minimum to a more stable minimum, through a saddle point. Hence, the existence of the saddle point and of the minima has to be well defined in the energy landscape. Therefore, the Néel-Brown expression for the relaxation rate is valid for  $\sigma$  ranging from a few units to a few tens, which is the case for the magnetic systems used in hyperthermia applications. The Néel-Brown formula reads

$$\tau_D \Gamma_0 = \frac{\sigma^{1/2} (1 - h^2)}{\sqrt{\pi}} \times \left[ (1 + h) e^{-\sigma(1+h)^2} + (1 - h) e^{-\sigma(1-h)^2} \right], \quad (17)$$

where  $h = x/2\sigma$  and  $\tau_D \sim 2 \times 10^{-10} - 2 \times 10^{-12}$  s is the free-diffusion time.

In the presence of (weak) DI, Jönsson and Garcia-Palacios<sup>20</sup> showed that the relaxation rate depends on the damping factor  $\lambda$  and is expressed as a quadratic function of the longitudinal and transverse components of the DI field  $\Xi_i$ . Accordingly, the explicit expression of  $\eta$  depends on the lattice through sums such as  $\mathcal{R} = 2 \sum_{j \neq i} r_{ij}^{-6}$ ,  $\mathcal{T} = \sum_{j \neq i} (\mathbf{e} \cdot \mathbf{D}_{ij} \mathbf{e})^2$ <sup>20,28</sup>. More precisely, we have

$$\eta = \frac{\omega}{\Gamma} = \frac{\omega}{\Gamma_0} \left[ 1 - \frac{\xi^2}{6} \mathcal{S}(\lambda) \right], \quad (18)$$

with  $\mathcal{S}(\lambda) = (1 + F(\lambda)) \mathcal{R} + (3\mathcal{T} - \mathcal{R}) (1 - F(\lambda)/2) S_2$ . The function  $F(\alpha)$  is given by<sup>29</sup>

$$F(\alpha) = 1 + 2(2\alpha^2 e)^{1/(2\alpha^2)} \gamma\left(1 + \frac{1}{2\alpha^2}, \frac{1}{2\alpha^2}\right), \quad (19)$$

where  $\gamma(a, z) = \int_0^z dt t^{a-1} e^{-t}$  and  $\alpha = \lambda\sqrt{\sigma}$ .

Finally, substituting in Eq. (10) the expressions (12, 13) or (14,15) for  $\chi^{\text{eq}}$  and (17, 18) for  $\Gamma$ , renders an expression of the AC susceptibility for the assembly in the presence of DI. Therefore, the DI contribute to  $\chi''$  through the relaxation rate as well as the equilibrium susceptibility. However, it can easily be seen that for low concentrations the DI correction is mostly brought in by the equilibrium susceptibility. Hence, to first order in  $\xi$  we can write  $(\eta_0 = \omega \Gamma_0^{-1})$ <sup>28</sup>

$$\chi'' \simeq \frac{\eta_0}{1 + \eta_0^2} \left[ \chi_{\text{free}}^{\text{eq}} + \xi \chi_{\text{int}}^{\text{eq}} \right]. \quad (20)$$

Note that this result agrees with Eq. (34) of Ref. 1 for  $\xi = 0$ . Indeed, the expression of  $\chi_{\text{free}}^{\text{eq}}$  given in Eq. (12) provides a clear basis for the phenomenological formula of Eq. (38) given by Carrey *et al.* In fact, the factor  $\frac{1}{3} \left( 3 - \frac{2}{1 + (\sigma/3.4)^{1.47}} \right)$  with *ad-hoc* exponents and coefficients is extracted from a fitting of the ratio  $\chi_{\text{free}}^{\text{eq}}/\chi_{\text{Langevin}}$ , supposedly with the aim to obtain an interpolation between the two regimes  $\sigma \ll 1$  and  $\sigma \gg 1$ . However, as we have already mentioned, for applications to hyperthermia we have the typical values of  $\sigma \simeq 5 - 30$ . In this case, analytical calculations show that it is a good approximation to replace the ratio  $\chi_{\text{free}}^{\text{eq}}/\chi_{\text{Langevin}}$



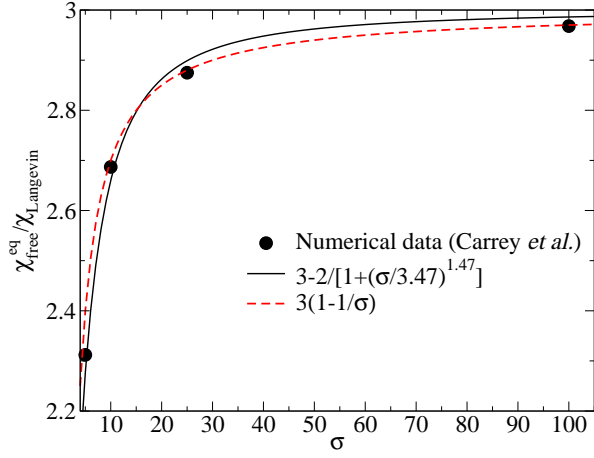


Figure 3.  $\chi_{\text{free}}^{\text{eq}}/\chi_{\text{Langevin}}$  as a function of the anisotropy parameter  $\sigma$ . The numerical data are extracted from Ref. 1 and are compared to the phenomenological expression  $(3 - \frac{2}{1+(\sigma/3.4)^{1.47}})$  and to the analytical expression  $3(1-1/\sigma)$ .

by  $(1-1/\sigma)$ , as can be seen in the square brackets in Eq. (12). This is clearly illustrated by the results in Fig. 3.

The DI parameter  $\xi$  defined in (8) can be rewritten in terms of the particles concentration  $C_v$  as<sup>24</sup>

$$\xi = \frac{\mu_0}{4\pi} \frac{m^2}{k_B T} \frac{C_v}{V}. \quad (21)$$

#### IV. SPECIFIC ABSORPTION RATE – EFFECT OF DC FIELD AND CONCENTRATION

##### A. SAR for “noninteracting assemblies”

Let us first examine the behavior of the SAR as a function of the applied DC field for noninteracting (*i.e.* free) particles. Within this approximation the SAR can be written as

$$\text{SAR} = \left(\frac{\mu_0}{2\pi}\right) \frac{\Gamma_0 \eta_0^2}{1 + \eta_0^2} H_0^2 \chi_{\text{free}}^{\text{eq}}. \quad (22)$$

In the case of a longitudinal ( $\parallel$ ) DC field, the expressions of  $\Gamma_0$  and  $\chi_{\text{free}}^{\text{eq}}$  are given in Eqs. (17) and (12) or (14), respectively. For a transverse ( $\perp$ ) DC field, the general expression of Eq. (22) still holds, one should simply replace the expression of the relaxation rate  $\Gamma_0$  and that of the free susceptibility by the appropriate expressions<sup>12,30</sup>, namely

$$\tau_D \Gamma_0^\perp = \frac{[1-2h+\sqrt{1+4\lambda^{-2}h(1-h)}]\sqrt{1+h}}{2\pi\sqrt{h}} e^{-\sigma(1-h)^2}, \quad (23)$$

$$\chi_{\text{free}}^{\text{eq},\perp} = \left(\frac{\mu_0 m^2}{k_B T}\right) \frac{1}{2\sigma} \frac{(1+h^2) \cosh x - 2h \sinh x}{(1-h^2)(\cosh x - h \sinh x)}.$$

Using these expressions one can see that the transverse susceptibility  $\chi_{\text{free}}^{\text{eq},\perp}$  only weakly depends on the DC field

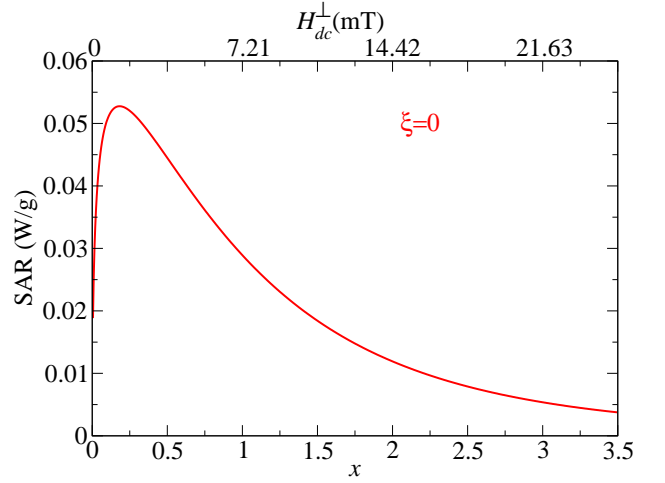


Figure 4. SAR as a function of the transverse DC magnetic field  $H_{\text{DC}}$  for  $H_0 = 7.3$  mT,  $\omega = 35.18 \times 10^4$  rad/s.

$x$ ; only 3% of change over the range  $x = 0 - 2$ . On the contrary,  $\chi_{\text{free}}^{\text{eq},\parallel}$  changes by an order of magnitude over the same range, as shown by the black dashed curve in Fig. 2. This explains why the effect of the DC field on the SAR is more pronounced in the longitudinal case. The effect of a transverse DC field on the SAR of non-interacting assemblies is shown in Fig. 4. Notice the scale on the vertical axis.

The results are presented for external DC fields below 25 mT. Indeed, we have to restrict ourselves to  $H_{dc}^\perp < H_K = \frac{2K_{\text{eff}}}{M_s} \simeq 77$  mT in order to preserve the picture of a two-well potential energy on which the over-barrier escape rate theory<sup>31,32</sup> is based.

In the sequel, we will focus on the longitudinal geometry where more pronounced effects are observed. This will be done in the presence of DI.

##### B. SAR for (weakly) interacting assemblies

In the absence of a DC magnetic field (*i.e.*  $x = 0$ ), we can use Eqs. (21, 20) together with Eq. (2) to write a relatively simple expression for the SAR of a (weakly) interacting assembly in terms of the particles concentration  $C_v$

$$\begin{aligned} \text{SAR} = & \left(\frac{\mu_0}{2\pi}\right) \frac{\Gamma_0 \eta_0^2}{1 + \eta_0^2} \left(\frac{\mu_0 m^2}{k_B T}\right) H_0^2 \left[\left(1 - \frac{1}{\sigma}\right) \right. \\ & \left. + \mathcal{C}^{(0,0)} \xi(C_v) \left(1 - \frac{2}{\sigma}\right)\right]. \end{aligned} \quad (24)$$

In particular, this expression shows that, to 1<sup>st</sup> order, the SAR is linear in the concentration of the assembly with a strong dependence on its shape via the coefficient  $\mathcal{C}^{(0,0)}$  [see discussion in Section V B].

We now consider the evolution of the SAR as a function of the DI parameter  $\xi$ , in a variable external DC magnetic field for which we introduce the new parameter  $h = x/2\sigma$ .

For numerical estimates, we have used the physical parameters of FeCo, the magnetic material studied in Ref. 16, namely  $M_s = 1.162 \times 10^6$  A/m,  $K_{\text{eff}} = 4.5 \times 10^4$  J/m<sup>3</sup> with a density  $\rho \simeq 8300$  kg.m<sup>-3</sup>. In SI units the SAR is expressed in Watt per particle but it is more commonly measured in W/g. We have also assumed that each nanoparticle is a sphere of radius  $R = 5$  nm. For such a size but elongated shape, which leads to a strong effective anisotropy, the blocking temperature of an individual particle is  $\sim 60$  K. However, the working temperature relevant to hyperthermia applications is  $T = 318$  K, leading to the reduced anisotropy-energy barrier  $\sigma \simeq 5.4$ . This implies that the individual nanoparticles are in the superparamagnetic state. This is an additional reason for which the SAR behavior is mostly dictated by the equilibrium susceptibility, as stressed earlier.

Regarding the AC magnetic field, we have set it at a small amplitude  $H_0 = 7.3$  mT so as to remain in the linear regime and to preserve the validity of the approach leading to Eq. (2) for the SAR. Indeed, we note that this amplitude is smaller than the usual experimental value, *e. g.* 23 mT, as in Ref. 17. As a consequence, since the SAR scales like  $H_0^2$ , the computed value in this paper should be at least one order of magnitude lower than that observed in experiments. In fact, as stressed earlier, our aim here is not to achieve a quantitative agreement with experiments regarding the SAR but rather to explain the role of DI and its possible competition with an external DC magnetic field. An extension of the present approach beyond the linear regime should be possible on the basis of the developments in Refs. 22, 23, and 33.

Then, using Eqs. (14,15) we obtain the expression for the SAR of the now (weakly) interacting assembly

$$\text{SAR} = \frac{\omega^2 \Gamma_0(h)}{\omega^2 + \Gamma_0^2(h)} \frac{\mu_0 H_0^2}{2\pi} \left[ \chi_{\text{free,GP}}^{\text{eq}} + \tilde{\chi}_{\text{int,GP}}^{\text{eq}} \right], \quad (25)$$

where the relaxation rate depends on the external DC field according to Eq. (17). Expression (25) is plotted in Fig. 5 against the variable  $X = 10^{-21}/a^3$ , where  $a$  is expressed in meters.

An interesting behavior is observed for oblate samples, as can be seen in the upper panel in Fig. 5, in the specific case of a two-dimensional square sample (depicted in Fig. 1). Here, the nano-spheres are placed on the vertices of a square lattice lying in the  $xy$ -plane, with their effective anisotropy axes parallel to the  $z$ -axis and the DC field applied parallel to the latter. In the present setup, there is a competition between the DI and the DC field. Consequently, the results in Figs. 5 and 6 show that there are two ways to enhance the SAR, namely by tuning either the concentration or the magnitude of the DC field.

The curve crossing seen in the upper panel in Fig. 5 can be understood upon analyzing the behavior of  $\chi^{\text{eq}}$  in the presence of DI, as shown in Fig. 2. Indeed, one clearly sees that for an inter-particle distance of 40 nm *i.e.*  $X \sim 15$ , the equilibrium susceptibility reaches a maximum for a DC field of about  $H_{\text{DC}}^{\text{max}} = \frac{k_B T}{m} x_{\text{max}} = \frac{k_B T}{m} 0.8 \simeq 6$  mT. According to Eq. (25), this means that the SAR should

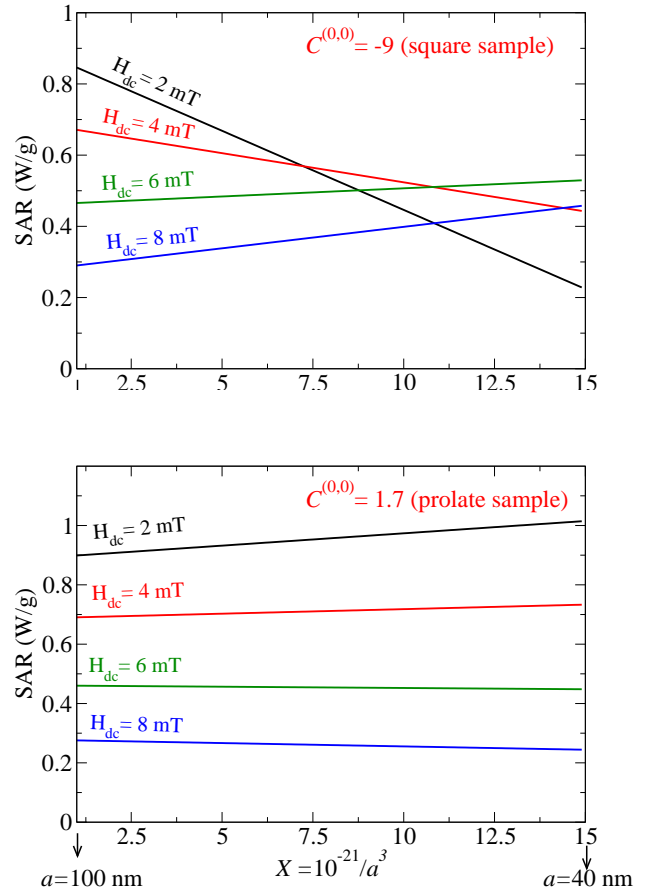


Figure 5. SAR as a function of  $X$  (see text) for various values of the longitudinal field  $H_{\text{DC}}$  with  $H_0 = 7.3$  mT,  $\omega = 35.18 \times 10^4$  rad/s.

exhibit a maximum around this field. However, this interpretation should take into account the fact that the SAR in Eq. (25) depends on  $h$  not only through the equilibrium susceptibility but also through the relaxation rate  $\Gamma_0(h)$ . In order to clarify the effect of the dynamics, let us now further focus on the effect of the DC field on the SAR. For this purpose, in Fig. 6 we plot the SAR as a function of the field, as rendered by Eq. (25). In Fig. 6 (a), we plot Eq. (25) where we have used the relaxation rate in zero field, *i.e.*  $\Gamma_0(h = 0)$ , which means that we simply adopt the Arrhenius law for the relaxation rate  $\Gamma_0$ . On the other hand, in Fig. 6 (b) we plot the full expression (25) where  $\Gamma_0(h)$  is given by Eq. (17). The idea here is to assess the contribution to the SAR of the DC magnetic field through the dynamics, or more precisely through the relaxation rate, and to compare it with that brought in by the equilibrium susceptibility. Accordingly, we see that the DC field  $h_{\text{max}}$ , at which the SAR reaches its maximum, is slightly shifted to higher values as the concentration increases. However, the qualitative overall behavior remains the same. This result implies that for the typical assemblies studied here, the overall behavior of the SAR is mainly governed by the equilibrium suscep-

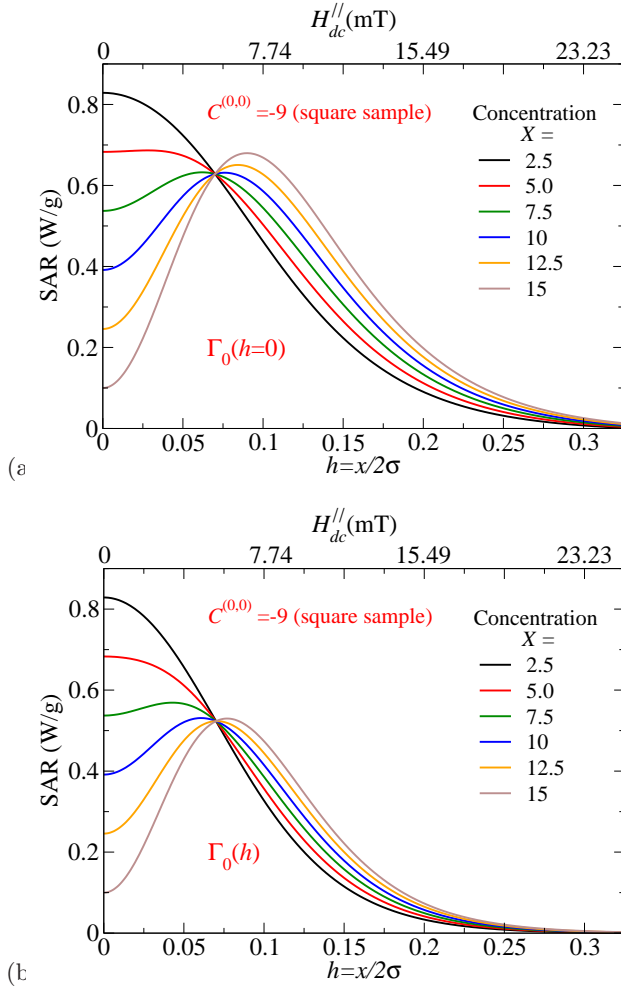


Figure 6. The SAR as a function of the longitudinal DC field for various values of the concentration  $X$ . (a) SAR obtained by setting  $h = 0$  in  $\Gamma_0$  in Eq. (25), (b) the SAR obtained from Eq. (25) for non zero field.

tibility  $\chi^{\text{eq}}$ . There is a further remark in order regarding the curves in Fig. 6 (b). At some particular value of the DC applied field ( $h_c \simeq 0.07$ ), the SAR turns out to be independent of the concentration. In fact, this occurs when the DI contribution to the susceptibility ( $\chi_{\text{int}}^{\text{eq}}$ ) vanishes and thereby Eq. (25) becomes independent of  $\tilde{\xi}$  (or the concentration). Hence, the exact expression of  $h_c$  can be obtained by solving  $\chi_{\text{int,GP}}^{\text{eq}}(x_c) = 0$ , or an approximation thereof at low field obtained from Eq. (13), leading to  $h_c \sim \frac{1}{4\sigma} (1 + \frac{1}{2\sigma}) \simeq 0.05$ .

## V. DISCUSSIONS

Now we discuss the main issue of the present work, namely the contributions of DI and DC magnetic field to the SAR of an array of magnetic nanoparticles. In particular, we discuss the role of the underlying superlattice, emphasizing its geometry and structure.

### A. Effect of the DC magnetic field on the SAR

Both in the transverse and longitudinal static (DC) magnetic field we find that the SAR exhibits a bell-like shape. However, in the transverse setup the ascending part of the curve is rather abrupt and thus occurs over a narrow range of low field values [see Fig. 4]. This is probably the reason why only the descending part is observed in experiments. For instance, in Ref. 19 the authors studied the possibility to increase heating with the help of a DC magnetic field in the transverse configuration. They measured a SAR that is decreasing with increasing DC field, as can be seen in their Fig. 4. Again, in Ref. 17 the authors studied the effect of a transverse DC magnetic field on the SAR of FeCo nanoparticle assemblies. The results in their Fig. 3 (b) show that the hysteresis area (or the SAR divided by the AC field frequency) is a decreasing function of the DC field. However, if one examines their results more closely in the low-field regime, it turns out that a nonmonotonic behavior of the SAR is observed: close to 3 mT, it seems that the area of the hysteresis grows before decreasing continuously. This is in agreement with the predictions of the present theoretical developments. However, further experimental investigations are required to clarify this behavior of the SAR.

On the other hand, the longitudinal setup renders a clearly nonmonotonic behavior of the SAR with a maximum at a DC field that falls well within the experimental range. The SAR can also be obtained by computing the area of the dynamic hysteresis loop obtained by cycling over the AC magnetic field, see Ref. 1 and references therein. In the case of an oblate geometry, the DI lead to an effective magnetic moment in the plane of the assembly. Then, in the low-field regime, as we increase the DC field, the projection of this magnetic moment (on the field direction) increases, because the net magnetic moment tilts out of the assembly plane, leading to a widening of the hysteresis cycle  $M(H_{AC})$  and thereby to an increase of the SAR. As the critical value of the DC field is reached (see discussion above) the DC field wins against the DI and the magnetization saturates. Consequently, the equilibrium susceptibility and thereby  $\chi''$  goes down to zero.

In Ref. 34 the authors used the matrix-continued-fraction method to study the effect of a DC magnetic field on the AC susceptibility of a nanoparticle in the macrospin approximation. In particular, the results in their Fig. 1 show that, in the low-frequency regime, which is relevant to the present work, the imaginary component of the AC susceptibility decreases as the DC field (denoted there by  $\xi_0$ ) is increased beyond unity. This is of course in agreement with the behavior we observe here in the high-field regime, *i.e.*  $h > h_c$ , or  $x > 1$  as can be seen in Fig. 2 in the behavior of the equilibrium susceptibility. In fact, the latter imposes its bell-like shape to the out-of-phase component of the AC susceptibility and thereby to the SAR.

## B. Effects of the assembly super-lattice shape and structure

In Eq. (11) enters the lattice sum  $\mathcal{C}^{(0,0)}$  leading to the effective DI parameter  $\tilde{\xi} \equiv \xi \mathcal{C}^{(0,0)}$ . For the 2D array of  $N$  particles considered here,  $\mathcal{C}^{(0,0)}$  is defined by<sup>15</sup>

$$\mathcal{C}^{(0,0)} = \frac{1}{N} \sum_{i=1}^N \sum_{j \neq i} \frac{3(e_{ij}^z)^2 - 1}{r_{ij}^3},$$

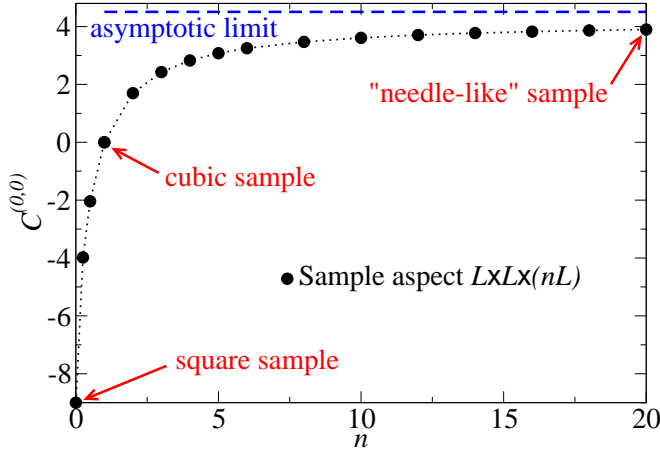


Figure 7. Systematic evaluation of the lattice sum  $\mathcal{C}^{(0,0)}$  as a function of  $n$  for  $N$ -particle samples with  $N = L \times L \times nL$ , note that  $n = 0$  means a 2D square sample.

easily be computed on the simple cubic lattice for samples with different shapes, with  $L_x = L$ ;  $L_y = L$ ;  $L_z = nL$ , by varying  $n$ . Namely,  $n = 0$  corresponds to a square sample,  $n = 1$  to a cubic sample, and if  $n \gg 1$  the sample assumes the shape of a needle. The results of the evaluation of  $\mathcal{C}^{(0,0)}$  at the thermodynamic limit are given in Fig. 7 and are summarized in the following Table:

$n$	$\mathcal{C}^{(0,0)} \approx$	$n$	$\mathcal{C}^{(0,0)} \approx$
0	-9.1	6	3.25
1/4	-3.98	8	3.47
1/2	-2.04	10	3.61
1	0	12	3.70
2	1.69	14	3.77
3	2.42	16	3.82
4	2.82	18	3.86
5	3.08	20	3.89

In order to highlight the competition between the applied field and the DI, we mainly focus on oblate samples. This implies that  $\mathcal{C}^{(0,0)} < 0$  and as it can be seen in Eq. (11), the sample aspect ratio plays a key role in the behavior of  $\chi^{\text{eq}}$ : while the role of the interactions is irrelevant for cubic samples since  $\mathcal{C}^{(0,0)} = 0$ , it gets more and more enhanced as one goes to planar samples as observed in Fig. 8.

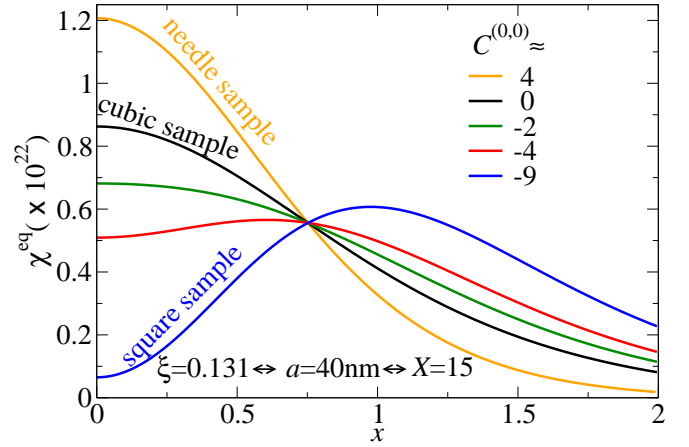


Figure 8. Equilibrium susceptibility given by Eqs. (11), (14) and (15) as a function of the DC field for samples with different aspect ratios:  $L \times L \times 20L$  (orange),  $L \times L \times L$  (black),  $L \times L \times \frac{L}{2}$  (green),  $L \times L \times \frac{L}{4}$  (red), and  $L \times L$  (blue).

As a consequence, the SAR changes from a bell-like curve (with a maximum) into a monotonously decreasing function of the applied DC field, as the sample passes from a pure 2D array into a thick slab and finally a “needle-like” sample. This means that the assembly shape plays a crucial role in the present approach. For the case of prolate samples, with  $\mathcal{C}^{(0,0)} > 0$ , the DC field does not compete with the DI, and both have the same effect on the anisotropy barrier, this translates into a decrease of the SAR as the DC field increases. In contrast, for the well controlled organized 2D arrays of nano-elements in vogue today (with  $\mathcal{C}^{(0,0)} < 0$ ), there is a competition between the DI and the DC field, such that the SAR should exhibit the bell-like shape.

## VI. CONCLUSION AND PERSPECTIVES

We have proposed a theoretical model and a practical tool for studying the qualitative behavior of the specific absorption rate of a monodisperse assembly of magnetic nanoparticles with oriented effective anisotropy, in the presence of dipolar interactions and a DC magnetic field, in addition of course to the AC field. We have dealt with both a longitudinal and transverse setup of the DC field with respect to the anisotropy axis. We have shown that, depending on the sample geometry, one can observe competing effects between the external DC field and the sample’s concentration (or equivalently the dipolar interaction). More precisely, in the case of oblate samples and for a given concentration, there is an optimal field magnitude that maximizes the specific absorption rate.

In the present work, we have modeled the magnetic state of the nanoparticles with the help of a macroscopic magnetic moment, thus ignoring their internal structure and intrinsic features, such as surface effects. In Ref. 35 the effect of surface anisotropy on the (static) hysteresis loop was investigated in the atomic approach with the



help of numerical methods. The same approach could be used to compute the dynamic hysteresis loops and thereby investigate the effect of surface and finite size on the specific absorption rate. The corresponding results could also be compared with the approach used here that uses the AC susceptibility upon extending it to the effective one-spin problem along the lines adopted in Ref. 28.

As mentioned earlier, the nonlinear regime with respect to the AC magnetic field should be studied upon generalizing the Debye model for AC susceptibility. An increase in the AC field affects the magnitude of the SAR explicitly through the prefactor and implicitly through the relaxation rate and the additional contributions from high frequency modes.

## ACKNOWLEDGMENTS

We would like to acknowledge instructive discussions with Oksana Chubykalo-Fesenko, David Serantes and Carlos Boubeta.

## REFERENCES

- <sup>1</sup>J. Carrey, B. Mehdaoui, and M. Respaud, *Journal of Applied Physics* **109**, 083921 (2011), 10.1063/1.3551582.
- <sup>2</sup>B. Mehdaoui, A. Meffre, J. Carrey, S. Lachaize, L.-M. Lacroix, M. Gougeon, B. Chaudret, and M. Respaud, *Advanced Functional Materials* **21**, 4573 (2011).
- <sup>3</sup>C. Haase and U. Nowak, *Phys. Rev. B* **85**, 045435 (2012).
- <sup>4</sup>C. Martinez-Boubeta, K. Simeonidis, A. Makridis, M. Angelakeris, O. Iglesias, P. Guardia, A. Cabot, L. Yedra, S. Estradé, F. Peiró, *et al.*, *Scientific reports* **3**, 1652 (2013).
- <sup>5</sup>I. Conde-Leboran, D. Baldomir, C. Martinez-Boubeta, O. Chubykalo-Fesenko, M. d. P. Morales, G. Salas, D. Cabrera, J. Camarero, F. J. Teran, and D. Serantes, *The Journal of Physical Chemistry C* **119**, 15698 (2015).
- <sup>6</sup>A. Kostopoulou and A. Lappas, *Nanotechnology Reviews* **4**, 595 (2015).
- <sup>7</sup>S. Ruta, R. Chantrell, and O. Hovorka, *Scientific Reports* **5**, 9090 (2015).
- <sup>8</sup>G. T. Landi, F. R. Arantes, D. R. Cornejo, A. F. Bakuzis, I. Andreu, and E. Natividad, *Journal of Magnetism and Magnetic Materials* **421**, 138 (2017).
- <sup>9</sup>R. Hergt, S. Dutz, R. Müller, and M. Zeisberger, *Journal of Physics Condensed Matter* **18**, 2919 (2006).
- <sup>10</sup>F. Ahrentorp, A. P. Astalan, C. Jonasson, J. Blomgren, B. Qi, O. T. Mefford, M. Yan, J. Courtois, J. Berret, J. Fresnais, O. Sandre, S. Dutz, R. Müller, and C. Johansson, *AIP Conference Proceedings* **1311**, 213 (2010).
- <sup>11</sup>R. Rosensweig, *Journal of Magnetism and Magnetic Materials* **252**, 370 (2002), proceedings of the 9th International Conference on Magnetic Fluids, 23-27 Jul. 2001.
- <sup>12</sup>J.L. Garcia-Palacios, "On the Statics and Dynamics of Magnetoanisotropic Nanoparticles," in *Advances in Chemical Physics*, Vol. 112 (John Wiley & Sons, Inc., 2007) pp. 1–210.
- <sup>13</sup>M. Azeggagh and H. Kachkachi, *Phys. Rev. B* **75**, 174410 (2007).
- <sup>14</sup>P. E. Jönsson and J. L. García-Palacios, *Phys. Rev. B* **64**, 174416 (2001).
- <sup>15</sup>H. Kachkachi and M. Azeggagh, *Eur. Phys. J. B* **44**, 299 (2005).
- <sup>16</sup>L.-M. Lacroix, R. B. Malaki, J. Carrey, S. Lachaize, M. Respaud, G. F. Goya, and B. Chaudret, *Journal of Applied Physics* **105**, 023911 (2009).
- <sup>17</sup>B. Mehdaoui, J. Carrey, M. Stadler, A. Cornejo, C. Nayral, F. Delpech, B. Chaudret, and M. Respaud, *Appl. Phys. Lett.* **100**, 052403 (2012).
- <sup>18</sup>L. C. Branquinho, M. S. Carrião, A. S. Costa, N. Zufelato, M. H. Sousa, R. Miotto, R. Ivkov, and A. F. Bakuzis, *Scientific Reports* **3**, 2887 EP (2013).
- <sup>19</sup>K. Murase, H. Takata, Y. Takeuchi, and S. Saito, *Physica Medica: European Journal of Medical Physics* **29**, 624 (2013).
- <sup>20</sup>P.E. Jönsson and J.L. Garcia-Palacios, *Europhys. Lett.* **55**, 418 (2001).
- <sup>21</sup>P. Debye, *Polar molecules* (Dover, 1929).
- <sup>22</sup>R. Zwanzig, *The Journal of Chemical Physics* **38**, 2766 (1963).
- <sup>23</sup>B. J. Berne, *The Journal of Chemical Physics* **62**, 1154 (1975).
- <sup>24</sup>Z. Sabsabi, F. Vernay, O. Iglesias, H. Kachkachi, *Phys. Rev. B* **88**, 104424 (2013).
- <sup>25</sup>A. Bakuzis and P. Morais, *Journal of Magnetism and Magnetic Materials* **226-230, Part 2**, 1924 (2001), proceedings of the International Conference on Magnetism (ICM 2000).
- <sup>26</sup>M. S. Carrião, V. R. R. Aquino, G. T. Landi, E. L. Verde, M. H. Sousa, and A. F. Bakuzis, *Journal of Applied Physics* **121**, 173901 (2017), <http://dx.doi.org/10.1063/1.4982357>.
- <sup>27</sup>A. Aharoni, *Phys. Rev.* **177**, 793 (1969).
- <sup>28</sup>F. Vernay, Z. Sabsabi, and H. Kachkachi, *Phys. Rev. B* **90**, 094416 (2014).
- <sup>29</sup>D.A. Garanin, E.C. Kennedy, D.S.F. Crothers, and W.T. Coffey, *Phys. Rev. E* **60**, 6499 (1999).
- <sup>30</sup>W. T. Coffey, D. S. F. Crothers, J. L. Dormann, L. J. Geoghegan, and E. C. Kennedy, *Phys. Rev. B* **58**, 3249 (1998).
- <sup>31</sup>J. S. Langer, *Phys. Rev. Lett.* **21**, 973 (1968).
- <sup>32</sup>W. Brown, *IEEE Transactions on Magnetics* **15**, 1196 (1979).
- <sup>33</sup>J. L. García-Palacios and D. A. Garanin, *Phys. Rev. B* **70**, 064415 (2004).
- <sup>34</sup>P.-M. Déjardin and Y. P. Kalmykov, *Journal of Magnetism and Magnetic Materials* **322**, 3112 (2010).
- <sup>35</sup>H. Kachkachi and M. Dimian, *Phys. Rev. B* **66**, 174419 (2002).